Stability of the Ketyl Radical as a Descriptor in the Electrochemical Coupling of Benzaldehyde

Journal:	*Catalysis Science & Technology*
Manuscript ID	CY-ART-02-2020-000282.R1
Article Type:	Paper
Date Submitted by the Author:	28-Mar-2020
Complete List of Authors:	Anibal, Jacob; University of Delaware, Chemical Engineering Malkani, Arnav; University of Delaware, Chemical Engineering Xu, Bingjun; University of Delaware, Chemical Engineering

SCHOLARONE™
Manuscripts

Stability of the Ketyl Radical as a Descriptor in the

Electrochemical Coupling of Benzaldehyde

Jacob Anibal, Arnav Malkani and Bingjun Xu*

Center for Catalytic Science and Technology, Department of Chemical and Biomolecular

Engineering, University of Delaware, 150 Academy Street, Newark DE, 19716

*bxu@udel.edu

Abstract

Electroreductive coupling is an emerging electrochemical pathway for the renewable upgrading of CO_2, CO and biomass derived oxygenates. In particular, electrochemical coupling of molecules with a carbonyl group has the potential to grow the molecular weight of substrates via C-C bond formation to produce valuable fuels and chemicals. However, a lack of mechanistic understanding hinders rational catalyst development for this coupling chemistry. In this work, the electrochemical reduction of benzaldehyde is employed as a model reaction to investigate the impact of four metals (Au, Cu, Pd and Pt) on the two carbonyl reduction pathways, i.e., direct electrochemical reduction to benzyl alcohol and reductive C-C coupling to a diol product, i.e., hydrobenzoin. Reactivity studies show that, of the metals tested, Cu has a unique ability to mediate the C-C coupling of benzaldehyde. Complementary in situ spectroscopic investigations suggest that this facilitation of C-C coupling is directly related to the ability of the Cu catalyst to stabilize a key reaction intermediate, i.e., the ketyl radical. Spectroscopic features of the ketyl radical are observed on Au and Cu surfaces at benzaldehyde reduction potentials, but not on Pd and Pt. A lower radical concentration for Au compared to Cu is likely the primary reason for the lack of C-C coupling on Au. On the Pd and Pt surfaces, CO formation is observed from the dissociative adsorption and decarbonylation upon benzaldehyde introduction, suggesting surface adsorbate instability under reducing conditions. From the combined reactivity and spectroscopic evidence, we propose that the ability of a catalyst to produce and stabilize the ketyl radical intermediate is a key descriptor in its ability to mediate the C-C coupling chemistry of aldehydes and ketones.

Introduction

Driven by the dropping cost of renewable electricity,[1] electroreductive coupling has recently emerged as a promising method for converting low value carbon-oxygenates into higher value fuels and chemicals. Perhaps the most prominent example of this upgrading is the electrochemical reduction of CO_2 and CO to C-C coupled products, such as ethanol, acetic acid, propanol, and ethylene.[2,3] Other organic species, however, can also undergo electroreductive coupling, including aldehydes, ketones and olefins.[4] Obtainable from biomass feedstocks, these compounds present a promising feedstock for the renewable production of higher molecular weight fuels and chemicals. Of particular interest are larger carbonyl compounds, such as phenyl and furanic carbonyls, derived from lignocellulosic biomass using fast pyrolysis,[5] and acid hydrolysis and dehydration,[6–8] respectively. Both have received renewed interest for upgrading by electrochemical reduction, although most recent work has focused on reduction to the alcohol or alkyl product.[9–13] Electroreductive coupling has been much less explored. Chadderdon et al. investigated the electrochemical reduction mechanism of furfural on Cu using electrochemical techniques and distance selective surface poisoning.[14] They suggest that furfural coupling occurs by an outer sphere process, away from the electrode, whereas the direct reduction products (alcohol and alkyl products) require direct surface contact. Diaz et al. took a more applied approach, performing furfural reduction in an anion exchange membrane flow system.[15] They demonstrate high conversion of furfural to the hydrodimer and suggest the importance of surface environment and/or pH in controlling furfural conversion and product selectivity. Despite these efforts, however, electroreductive coupling of carbonyls still lacks mechanistic understanding on the molecular level. In particular, the effect of the catalyst on dimerization selectivity is well-known,[4] but the underlying cause remains largely unexplained. Electrochemical benzaldehyde reduction

offers an effective model system to investigate this catalyst effect given its well established mechanism and relative simplicity.

First studied by Kaufman and Law[16–19] at the turn of the 20th century, interest in benzaldehyde reduction has recently reemerged due to the work of Song et al.,[20] with subsequent work by others at Pacific Northwest National Laboratory.[21–24] The electrochemical reduction of benzaldehyde is generally considered to go through two reduction pathways[25] (Scheme 1), although further reduction to toluene has also been reported at low pH on Pt and Pd.[26] In the first pathway, often termed electrocatalytic hydrogenation, benzaldehyde undergoes a direct two electron reduction to form benzyl alcohol. In the second pathway, typically termed dimerization or hydrodimerization (C-C coupling), two benzaldehyde molecules undergo one election reductions and recombine to form the hydrobenzoin dimer. Other furanic and aromatic aldehydes and ketones undergo similar reduction pathways.[14,25,27–33] Both reduction pathways are suggested to proceed through a ketyl radical or radical anion intermediate (depending on pH and solvent),[25] as evidenced by the two distinct reduction waves observed polarographically[34–39] and in the benzaldehyde CV on Pb.[40] An acid-catalyzed electron transfer disproportionation has also been suggested for reduction at high pH.[38] The relative selectivity of the two reduction pathways varies extensively depending on the electrode potential, pH, and catalyst (metal or glassy carbon) chosen.[17,20,40–42] The catalyst in particular has a large impact on the benzaldehyde reduction products, with distinct differences in coupling ability. In addition to Hg,[34–38,43] perhaps the most well studied catalyst is Pb,[40,44–46] which shows both reduction pathways, favoring the dimer at lower over potential and higher pH.[40] The dimer has also been observed on Zn,[47] Sn,[47] Ti,[41] and glassy carbon.[42] Recent work also suggests dimer formation on Co and Cu, although the extent of dimerization remains unclear due to interference by the carbon support.[24] In contrast to these

catalysts, however, the work of Song et al.[20] for benzaldehyde reduction on Pt group metals (Pt, Pd, Rh, Ni) shows only the alcohol produced, with no dimer species.[20] A similar alcohol selectivity has also been reported for Ni[48] and Raney Ni electrodes.[49] Although recent work has suggested dimerization on Ni is possible with an alcohol co-solvent and higher benzaldehyde concentrations.[23,24] Additionally, benzaldehyde reduction on Ag cathode shows near complete selectivity toward the alcohol.[50] Combined, these reduction demonstrations suggest a distinct difference between catalysts able to catalyze benzaldehyde coupling and those which cannot, and similarly sharp distinctions have also been observed for other aldehydes and ketones.[4] Yet, despite these extensive demonstrations, the reason for the different carbonyl coupling abilities of different catalysts still remains poorly understood.

In this work, we seek to improve this understanding by investigating the effect of different metals on the electrochemical reduction of benzaldehyde using a combination of reactivity and operando spectroscopic investigations. We perform benzaldehyde reactivity tests on Pd, Pt, Cu, and Au foils, and show Cu to have a unique benzaldehyde coupling ability among the four metals tested. Subsequently, we employ attenuated total reflection surface enhanced infrared reflection absorption spectroscopy (ATR-SEIRAS) to probe the catalyst surfaces in operando during reduction. We observe a ketyl radical intermediate and reduction products on the Au and Cu surfaces, with a higher radical concentration for Cu. In contrast, the Pd and Pt surfaces form large quantities of CO poison due to decarbonylation of unstable benzaldehyde surface intermediates. Combining the spectroscopic work and reactivity results, we propose that the ability of Cu to perform benzaldehyde coupling results from an optimum stabilization of ketyl radical intermediates, and that ketyl radical stability offers a reliable predictor for the C-C coupling activity of different metals for carbonyl species.
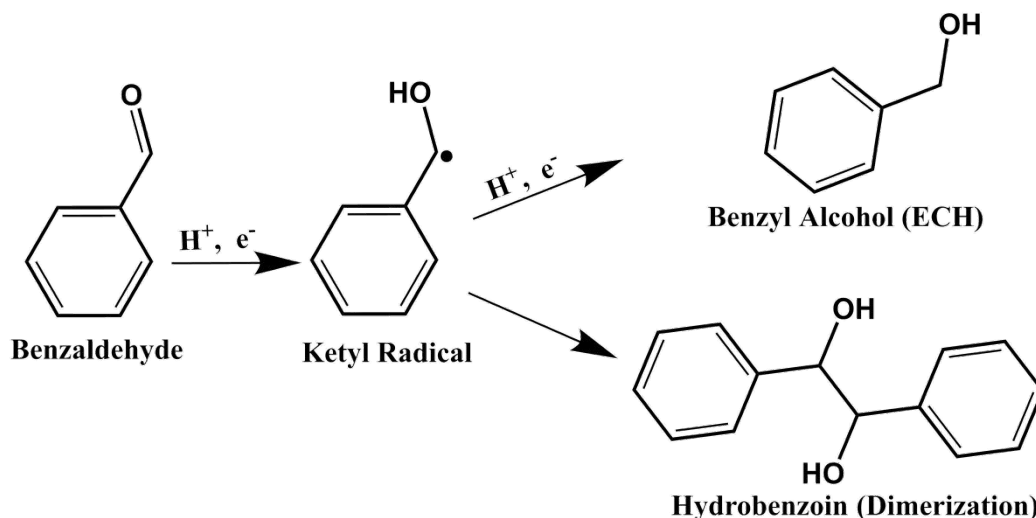
Scheme 1. Electrochemical benzaldehyde reduction pathways. ECH stands for electrocatalytic hydrogenation.

Results and Discussion

Reactivity Tests of the Electrochemical Reduction of Benzaldehyde

Batch electrochemical reactivity experiments are performed at -0.2 and -0.5 V (all potentials in this work are referred to the reversible hydrogen electrode (RHE), unless noted otherwise) in 0.5 M NaH_2PO_4 electrolyte (pH = 4.6) to evaluate benzaldehyde reduction activity and Faradaic efficiency (FE) on four different metal foil catalysts (Figures 1 and S1). Benzyl alcohol and hydrobenzoin are detected as the major products, with Cu producing additional trace side products at -0.5 V (see below). All metals show some decrease in reduction current with time, although it is most substantial for Pt and Pd at -0.5 V (Figure S2). At low overpotential (-0.2 V), Pt and Pd show exclusively electrocatalytic hydrogenation of benzaldehyde to benzyl alcohol, with hydrogen as the only side product. Pd shows a benzyl alcohol production rate of 0.83 μmol/h-cm^2 at -0.2 V (normalized by the geometric area of the metal foil), lower than the 4.38 μmol/h-cm^2 reported by Song and coworkers for Pd nanoparticles (rate normalized by CO chemisorption

area).[20] In contrast, the Pt foil shows a slightly higher benzyl alcohol rate of 1.59 µmol/h-cm^2

compared to the 0.82 µmol/h-cm^2 for Pt particles.[20] Au and Cu show no detectable activity for

benzaldehyde reduction at -0.2 V, with only trace amounts of hydrogen produced. The low overall

FEs at -0.2 V for Au and Cu result from the concentrations of products being too small to quantify

accurately. Reduction at -0.5 V does not significantly affect the product distribution for Pd or Pt,

but does increase the reduction rates by factors of ~12 and ~3, respectively (Figure 1A). This

potential dependence supports an electrochemical reduction, although the exact mechanism is not

inherently clear, as the reduction on Pt and Pd could proceed through an inner shell hydrogen

transfer instead of the sequential reductions suggested for other metals (Scheme 1). To investigate

this possibility, reduction control experiments are performed using hydrogen gas instead of an

electrochemical potential. Hydrogen gas is introduced to saturate the benzaldehyde solution and

the resulting H$_2$ saturated benzaldehyde solution allowed to react at the Pt and Pd electrodes for

one hour (Figure S3). Neither the Pt nor Pd foil shows any benzyl alcohol production after one

hour. To evaluate longer times, the Pt test is allowed to proceed for 40 h, resulting in a small

amount of benzyl alcohol. The ability of Pt to hydrogenate benzaldehyde without an applied

potential suggests that Pt, and likely Pd, can reduce benzaldehyde via an inner sphere hydrogen

transfer, in agreement with Song *et al*.[13] However, such a process appears much slower than the

electrochemical hydrogenation at room temperature, and is unlikely to dominate under the

electrochemical conditions employed in this work. Thus, a proton coupled electron transfer

(PCET) pathway appears more likely than hydrogen transfer for the electrochemical reduction of

benzaldehyde on Pt and Pd. This prominent non-hydrogen transfer pathway agrees with the

different electrochemical and thermochemical reduction mechanisms previously suggested by a

lower activation energy for electrochemical reduction.[13] Despite the lack of a hydrogen transfer,

the PCET mechanism has also been suggested as inner sphere, based on reaction orders and the decrease in hydrogen reduction activity upon benzaldehyde introduction.[13] At -0.5 V, Cu and Au also become active for benzaldehyde reduction. Au shows a strong preference for benzyl alcohol at 19% FE, with only negligible selectivity for the dimer (< 0.2%). Cu deviates from the other metals with a high selectivity for hydrobenzoin (FE = 37%, Figure 1B), in addition to benzyl alcohol (FE = 31%). A hydrobenzoin production rate of 19.5 μmol/h-cm^2 is observed on Cu at -0.5 V. The unique benzaldehyde coupling ability of Cu is reminiscent of its capability to promote C-C coupling in the electrochemical reduction of CO and CO_2.[51] In addition to hydrobenzoin, trace amounts of diphenyl acetaldehyde and deoxy-hydrobenzoin are also detected on Cu. Both species are hydrobenzoin isomers and likely form due to hydrobenzoin rearrangement, and not as primary reduction products or intermediates. Traces of diphenyl acetaldehyde are also observed in a control sample of 1 mM hydrobenzoin in phosphate buffer after three months (Figure S4A). No deoxy-hydrobenzoin is detected, however, suggesting that the rearrangement may benefit from a higher near electrode concentration during the reactivity test. In addition to these minor side products on Cu, both Pd and Cu show significant additional Faradaic losses at -0.5 V. Low FE for reactions on Pd is likely due to bulk hydride formation.[52,53] Control reactivity tests on Pd in pure buffer (without benzaldehyde) result in < 10% FE for H_2, while all other metals show > 85%. In contrast, Cu does not form a significant hydride phase, but a slightly lower overall FE is observed on Cu (81%) during benzaldehyde reduction at -0.5 V compared to Pt and Au (95-101%). The Faradaic loss likely results from the formation of oligomers via multiple C-C coupling reactions, or underestimation of hydrobenzoin due to strong adsorption to the Cu surface. To test these hypotheses, a spent Cu electrode is soaked in diethyl ether for 5 days after a -0.5 V run to solubilize adsorbed hydrobenzoin and/or the oligomers, and the supernatant solution analyzed with NMR

(Figure S4B). The NMR spectrum shows a strong, broad peak in the phenyl hydrogen region (6.7-7.8 ppm), likely corresponding to oligomers, and smaller, sharper peaks corresponding to hydrobenzoin, suggesting a contribution from both proposed causes of Faradaic loss. Similar oligomerization has previously been observed for the electrochemical reduction of furfural on Cu[54] and presents practical fouling difficulties for benzaldehyde reduction over long time periods. However, the benzaldehyde oligomerization does not appear quite as extensive as furfural, given the formation of ether soluble oligomers compared to the black carbonaceous product formed by furfural.[54] Recently, May and Biddinger have suggested mitigation strategies for the electrochemical fouling of furfural on Cu,[55] mainly the use of lower reactant concentrations and/or an organic co-solvent. These recommendations may also help reduce oligomerization for benzaldehyde on Cu. The co-solvent effect may also explain the reported lack of catalyst deactivation in some studies of benzaldehyde reduction on Cu in water-isopropanol mixtures.[21,24]
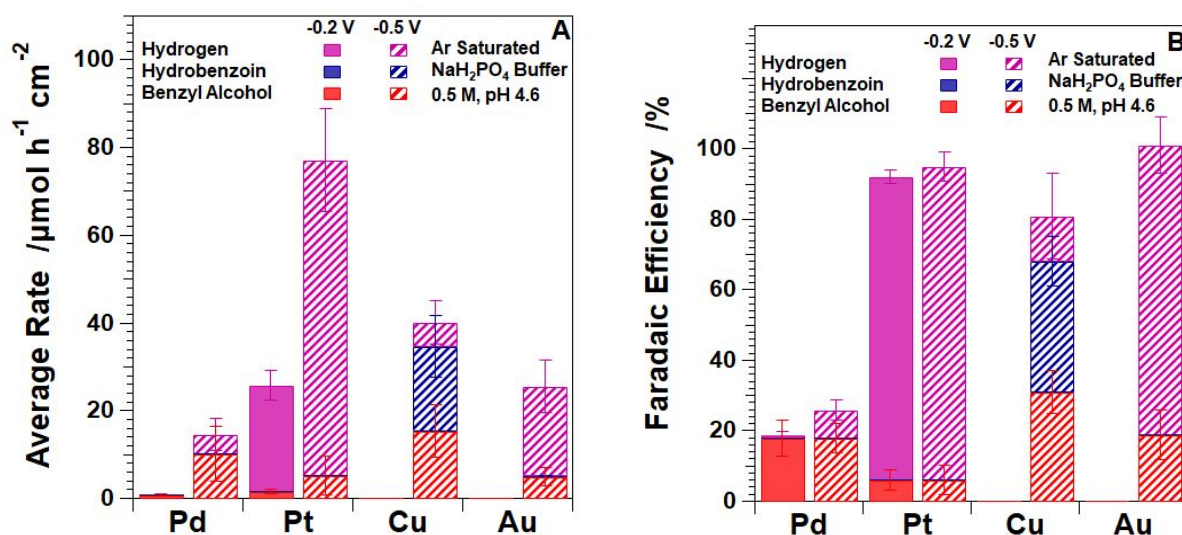

Figure 1. (A) Average production rates for hydrogen, hydrobenzoin, and benzyl alcohol on Pd, Pt, Cu, and Au metal foils at -0.2 and -0.5 V for 1 h. **(B)** The corresponding Faradaic efficiencies. All reactions occurred in Ar saturated 0.5 M NaH_2PO_4 solution (pH = 4.6) with 20 mM benzaldehyde.

ATR-SEIRAS Investigations of Benzaldehyde Reduction on Au and Cu Surfaces

To understand the adsorption and reaction pathway of benzaldehyde on the metal surfaces, operando ATR-SEIRAS is employed to probe the adsorption configuration and identify reaction intermediates. Benzaldehyde is introduced to the spectroscopic cell with a Au film working electrode at an initial concentration of 1.5 mM, followed by a gradual increase in the concentration to 24 mM (Figure 2A). Upon benzaldehyde introduction, vibrational bands appear at 1598, 1586, 1455 and 1310 cm^{-1}, corresponding to the ν_{8a}, ν_{8b}, ν_{18b} and ν_3 in-plane, ring stretching modes of benzaldehyde, respectively[56] (see Tables S1-S3 for a summary of peak assignments). We note that peak positions typically vary by < 2 cm^{-1} in experiments under identical conditions. As expected, the intensity of these bands increases with the benzaldehyde concentration. The 1694 cm^{-1} band corresponds to the C=O stretching mode of the benzaldehyde carbonyl group and is redshifted by 5 cm^{-1} compared to benzaldehyde in the bulk electrolyte collected with a bare Si ATR crystal (Figure S5A, no surface enhancement effect or potential). A similar red shift in the carbonyl has previously been observed for benzaldehyde on Pd particles and assigned to adsorbed benzaldehyde.[57] The stronger carbonyl shift compared to other bands suggests a stronger interaction, and the benzaldehyde likely adsorbs via the carbonyl carbon. Such binding likely occurs by back donation from the metal to the carbonyl π^* antibonding orbital. We note that the small red shift suggests a relatively weak interaction, which is consistent with the lack of the Stark tuning effect discussed below. Thus, the carbonyl group in benzaldehyde interacts with the surface via a mode that is between specific adsorption and physisorption. The carbonyl peak also shows a shoulder at ~1700 cm^{-1} corresponding to the bulk species, in agreement with the 1699 cm^{-1} carbonyl peak for the bulk species (Figure S5A). The relative size of the shoulder increases with benzaldehyde concentration, suggesting that benzaldehyde is preferentially adsorbed on the

electrode surface at low concentrations. The small peak at 1492 cm^{-1} which appears with the addition of benzaldehyde is attributed to a small amount of contaminant benzoic acid[58] formed via the oxidation of benzaldehyde upon air exposure.[59] To confirm whether the observed benzaldehyde peaks correspond to surface species, an additional set of spectra were collected using S-polarized light (Figure S5B). For sufficiently large islands, S-polarization eliminates surface enhancement, leaving only signals from bulk species.[60–63] No peaks appear upon benzaldehyde introduction with S-polarized light, suggesting the benzaldehyde is either surface adsorbed or very near the Au surface.
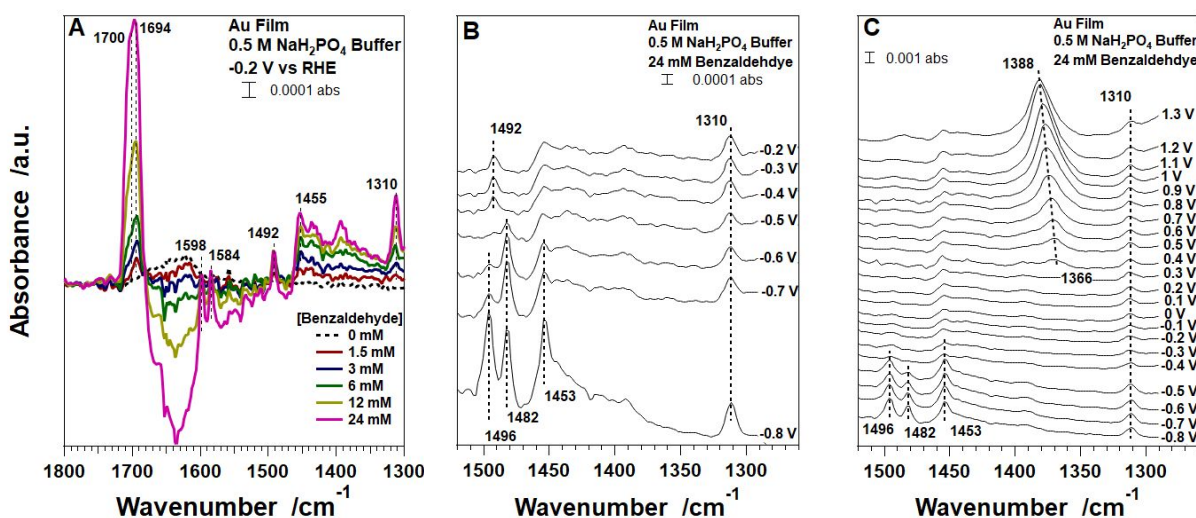

Figure 2. (A) ATR-SEIRAS spectra collected upon benzaldehyde introduction to the Au surface. **(B)** Spectra collected during cathodic potential steps on Au. **(C)** Spectra collected for Au during anodic potential steps. (B) and (C) were collected with 24 mM benzaldehyde. All spectra were collected in Ar purged solution with 64 co-averaged scans. Backgrounds were collected at -0.2 V in the absence of benzaldehyde.

A spectroscopic feature corresponding to the ketyl radical intermediate is identified on Au at reducing potentials, supporting the involvement of a radical intermediate in the electrochemical reduction of benzaldehyde. After benzaldehyde introduction, the potential of the Au surface is stepped down to -0.8 V in 0.1 V increments, with spectra collected at each potential. The spectra show no detectable shift in the position of any benzaldehyde band with potential (Figures 2B and

S6). In contrast, the OH bending mode of interfacial water at 1630-1650 cm^{-1} clearly shifts with

potential (Figure S6). The lack of Stark tuning for benzaldehyde suggests weak adsorption with

the carbonyl bond outside the inner Helmholtz layer, as this region contains the strong electric

field required for the Stark tuning.[64] This distance has been suggested as 2.5 – 4 Å in previous

Stark tuning studies,[64,65] in agreement with the ~4 Å double layer thickness estimated by surface

x-ray scattering studies of cations.[66,67] This adsorption distance (2.5 - 4 Å) may allow sufficient

surface interaction for electrochemical reduction without a Stark tuning effect. Recent

computational work has suggested electrochemical benzaldehyde reduction requires an adsorption

distance less than 4 Å.[68] The adsorption distance also generally agrees with those suggested for

larger organics both experimentally[69–71] and by computational modeling.[72] Unfortunately, the

current ATR-SEIRAS spectra do not provide sufficient information to determine an exact

adsorption distance. Other methods such as normal incident x-ray standing wave

spectroscopy[69,70,73,74] or atomic force microscopy[71] might allow for a more precise determination

of adsorption distance. In addition to benzaldehyde, other vibrational bands appear below the onset

potential of benzaldehyde reduction at -0.5 V. Of these bands, the peaks at 1496 and 1453 cm^{-1}

correspond to benzyl alcohol and appear prominently at lower potentials (E < -0.7 V). These peaks

agree with bulk benzyl alcohol spectra collected in a control experiment on a bare Si (Figure S5A),

with the stronger 1453 cm^{-1} peak differentiating them from those of hydrobenzoin. The benzyl

alcohol prominence agrees with the high benzyl alcohol selectivity observed in the reactivity test

at -0.5 V. In addition to benzyl alcohol, a third peak at 1482 cm^{-1} emerges at -0.5 V and grows in

intensity at more negative potentials. This peak does not correspond to benzaldehyde, benzyl

alcohol, or hydrobenzoin.[56,58] The emergence of this peak at a higher potential (-0.5 V) than peaks

corresponding to benzyl alcohol (≤ -0.6 V) suggests that it likely belongs to a reaction intermediate,

i.e., the benzaldehyde ketyl radical as suggested by previous electrochemical studies.[40,46,75] We note that benzyl alcohol is produced at -0.5 V on Au in the reactivity test (Figure 1), while the spectra show no discernable alcohol peak at this potential. The discrepancy likely results from the different time scales of the two experiments, as the one hour reactivity tests allow the accumulation of benzyl alcohol in the bulk, which may be detected even for steady state surface concentrations below the IR detection limit. Additional support for the radical assignment also comes from the peak position. Vibrational bands near 1482 cm^{-1} have previously been attributed to other ketyl radicals. Tallant and Evans attributed bands at 1500 cm^{-1} and 1375 cm^{-1} to radical anions of p-benzoquinone and benzophenone, respectively (without specifying the vibrational mode).[76] In multiple reports, Eargle and coworkers have reported redshifts of 80-120 cm^{-1} for ketyl radicals relative to their carbonyl stretch,[77–79] making the assignment of the 1482 cm^{-1} band to the ν(C-O) mode of the ketyl radical unlikely, as it would represent a > 200 cm^{-1} redshift compared to the benzaldehyde carbonyl vibration. More likely, the 1482 cm^{-1} peak corresponds to a ring stretching mode of the radical species, similar to the benzyl alcohol band at 1496 cm^{-1}, which is consistent with the assignment of a 1458 cm^{-1} band to a ring mode of the radical anion of benzophenone by Bewick et al.[80] The same authors also observed a band at 1557cm^{-1} corresponding to the ν(C-O) mode of the benzophenone ketyl radical. For the benzaldehyde ketyl radical, this mode could be obscured by the strong δ(OH) mode of water at 1630-1650 cm^{-1}.

SEIRA spectra collected during anodic potential steps on Au further support the assignment of the 1482 cm^{-1} band to the ketyl radical species. The 1482 cm^{-1} band decreases in intensity as the potential becomes more positive from -0.8 V and disappears above -0.5 V (Figure 2C), consistent with the spectra collected during the cathodic potential steps. The disappearance of the 1482 cm^{-1} band suggests that it corresponds to a reactive species produced at negative

potentials, consistent with the assignment to the ketyl radical. In contrast, the 1496 and 1453 cm^{-1} bands corresponding to benzyl alcohol linger, albeit weakened, at potentials above -0.4 V, suggesting that it is a stable species produced at negative potentials which diffuses from the double layer at more positive potentials. For the 1482 cm^{-1} band, alternative assignments should also be considered, particularly those related to surface pH. Given the reactions at the Au surface, the local pH might increase and result in new peaks for pH dependent species, such as acetals or deprotonated species. To rule out these possibilities, spectra are also collected for benzaldehyde at the Au surface in 0.1 M NaOH (Figure S7). The spectra in NaOH show benzaldehyde peaks, but lack the peak at 1482 cm^{-1}, suggesting this peak results from an electrochemical reduction intermediate rather than a pH change. While stepping the electrode potential up from -0.8 to 1.3 V, a new 1366 cm^{-1} band also appears above 0.4 V and shifts to higher wavenumber with potential at a Stark tuning rate of 24 cm^{-1}/V (Figure 2C). This peak is attributed to adsorbed benzoate.[81] The low onset potential of this peak suggests an initial adsorption of trace benzoic anions present due to benzoic acid impurity in the benzaldehyde. The further growth in the adsorbed benzoate band with potential likely results from additional benzoate coverage due to the oxidation of benzaldehyde.

The Cu surface shows different spectral features than Au, consistent with the higher C-C coupling activity of Cu in benzaldehyde reduction. Similar to Au, characteristic benzaldehyde bands appear upon introduction of benzaldehyde to the electrolyte at -0.2 V hold (Figure S8). In particular, the adsorbed carbonyl appears at 1695 cm^{-1}, with a 1702 cm^{-1} shoulder, suggesting weak adsorption of benzaldehyde to the Cu surface. Upon stepping down the potential, no new spectral features are observed between -0.2 and -0.4 V, consistent with the lack of benzaldehyde reduction at -0.2 V in the reactivity study (Figure 1A). At -0.5 V, however, many new bands appear (Figure

3A) and grow with time (Figures 3B, S9 and S10A), suggesting new chemistries upon reduction onset. The peaks at 1963, 1897, 1807, 1604, 1496, 1455, 1191, 1080 and 1022 cm^{-1} correspond to hydrobenzoin,[58] although some ring modes appear shifted $\pm$ 15 cm^{-1} compared to the bulk spectra.[58] Such shifts have been observed previously for adsorbed benzene derivatives,[82] and may suggest greater interaction of the hydrobenzoin rings with the Cu surface. Unfortunately, a comparison with bulk hydrobenzoin could not be made, as hydrobenzoin has a low solubility in water ($\leq$ 1mM), and no detectable bands are observed for a bare Si ATR crystal in hydrobenzoin saturated buffer. The high intensities of the observed hydrobenzoin bands on Cu at -0.5 V suggest a higher concentration in the double layer than its solubility limit in the bulk, likely due to stronger adsorption. This strong adsorption could result in slow diffusion of the produced hydrobenzoin from the surface and enhance further reaction to less soluble products via oligomerization. The strong adsorption and oligomerization are consistent with the detection of deposits on the spent Cu catalyst (Figure S4B) and the observed Faradaic loss during reactivity tests (Figure 1B). In addition to hydrobenzoin, a small, sharp peak is also present around 1673 cm^{-1} (Figure S9). This 1673 cm^{-1} peak could correspond to the ν(C-O) mode of the ketyl radical, which is likely obscured by the water band in the spectra on Au. The relatively small redshift of this mode from the benzaldehyde carbonyl band ($\sim$25 cm^{-1}), as compared to those reported for benzophenone and benzil (85-110 cm^{-1}),[76] could result from additional interactions in the aqueous system not present in the previous aprotic solvents.[76–79] For example, the band may be influenced by short range interactions with water molecules, such as hydrogen bonding. Such short range interactions have been suggested for the benzaldehyde ketyl in polar solvents, such as methanol or ethanol, resulting in charge transfer complexes.[83] Although, to our knowledge, such complexes have not been investigated experimentally. The aqueous environment could also interact via protonation of the ketyl radical.

Given the pKa estimate of 8-9 for the ketyl radical in water,[84] the majority of radicals should be protonated in the pH 4.6 phosphate buffer. Either interaction could serve to withdraw electron density from the ketyl radical and result in a smaller aldehyde to ketyl shift, as carbonyl electron density generally correlates inversely with ketyl radical peak position.[79] Alternatively, the lower shift could result from the different bonding structures of the respective radicals. Previous electron spin resonance measurements suggest a rigid C-C bond between the aldehyde and phenyl group for the benzaldehyde ketyl,[85,86] whereas that of benzophenone can rotate freely.[86,87] This rigid bond may suggest more sp2 character for the benzaldehyde ketyl radical, resulting in a higher vibrational frequency. Likely, both the additional water interactions and different bonding character could play a role in explaining the lower shift. However, the current spectra do not provide enough information to establish a predominant effect. Unfortunately, the large hydrobenzoin peak on Cu at 1496 cm^{-1} obscures the other likely ketyl radical peak expected near the 1482 cm^{-1} peak of Au. The stronger radical and hydrobenzoin bands on Cu suggest stronger coupling activity and higher activity overall, in agreement with the activity tests. In addition to hydrobenzoin and the ketyl radical, weak peaks at 1328, 1344, 1299, 1258, 1277, and 1220 cm^{-1} also appear on Cu at -0.5 V, which likely correspond to the trace hydrobenzoin rearrangement products observed in the Cu reactivity studies. A monotonic decrease in the intensity of all bands is observed as the electrode potential decreases from -0.5 to -0.9 V, which is likely due to the increasing coverage of the surface by oligomerized compounds or film damage due to strong hydrogen bubble formation.
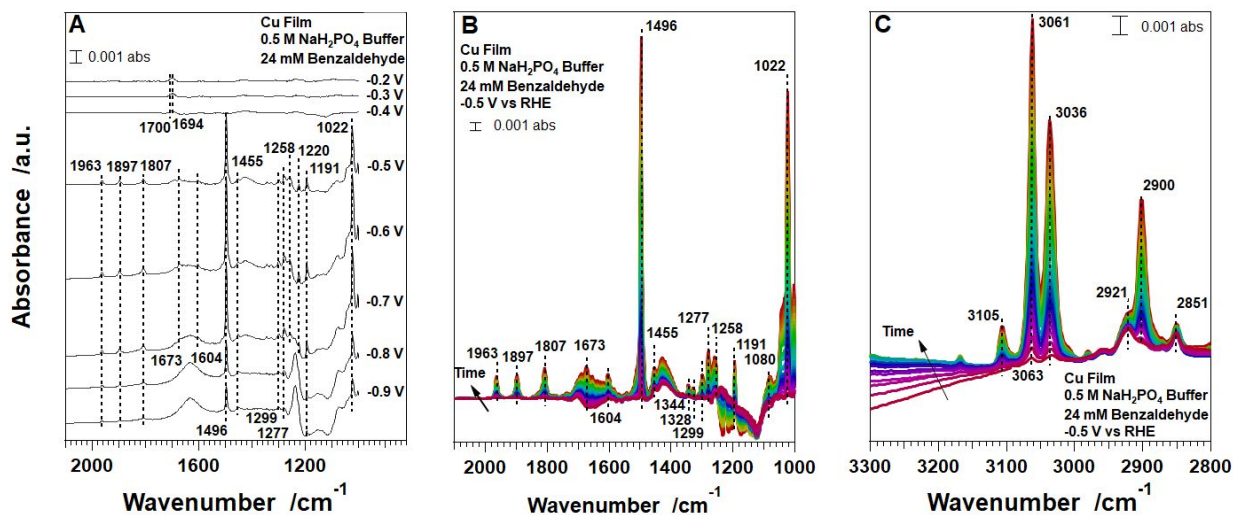
Figure 3. (A) ATR-SEIRAS spectra collected during cathodic potential steps on Cu. Each trace represents the final spectrum collected at the stated potential. **(B)** Time evolution spectra for the Cu surface upon stepping to -0.5 V. Spectra were collected ~ 3 min apart. **(C)**. The C-H stretching region of the same time evolution spectra in (B). All spectra were collected in Ar purged solution with a benzaldehyde concentration of 24 mM. Backgrounds were collected at -0.2 V without benzaldehyde.

The time evolution of C-H stretching modes of the species produced on Cu at -0.5 V provides further insight into the C-C coupling mechanism. In addition to the lower frequency bands, well-defined bands corresponding to v(C-H) modes are observed on Cu at -0.5 V. Such bands are too weak to distinguish on Au at the same potential, further supporting the high surface coverage of benzaldehyde derived compounds on Cu. Bands at 2921 and 2851 cm^{-1} correspond to benzyl alcohol[58] and appear immediately after reaching reduction onset at -0.5 V (Figures 3C and S10B), followed by the gradual growth of bands at 3061, 3036 and 2900 cm^{-1} corresponding to hydrobenzoin. The slower hydrobenzoin formation agrees with the time evolution spectra of the lower wavenumber range, in which the benzyl alcohol bands at 1496 and 1454 cm^{-1} appear in the first spectrum at -0.5 V, followed by the gradual appearance of the bands corresponding to hydrobenzoin (Figures 3B and S10A). The peak at 3105 cm^{-1} does not belong to either benzyl alcohol or hydrobenzoin.[58] Given its relatively large size, and co-emergence with hydrobenzoin, the peak likely relates to the ketyl radical species. The spectra also show a two small peaks at 3167

and 2980 cm^{-1} which emerge at longer times. Similar to the small peaks observed in the 1000 - 1800 cm^{-1} region, these peaks also likely correspond to trace side products from hydrobenzoin rearrangement. The sequential growth of the benzyl alcohol band and hydrobenzoin bands suggest coupling to hydrobenzoin occurs only after sufficient radical accumulation near the surface, with a lower concentration required for benzyl alcohol. This hypothesis is consistent with the observation that the 1673 and 3105 cm^{-1} bands assigned to the ketal radical also grow in sync with the other hydrobenzoin bands (Figures 3B, 3C and S10). The requirement for a high ketyl radical concentration may also explain the difference between Cu and Au. The Au spectra also show the ketyl radical, but do not show any hydrobenzoin formation spectroscopically, and produce only trace dimer (< 0.2%) in the reactivity studies (Figures 1 and 2). The lack of any substantial hydrobenzoin production, despite ketyl radical formation, suggests that the dimer is not favored on Au due to a low concentration of ketyl radicals. This low concentration likely results from the weaker stabilization of the ketyl radical intermediate by the Au surface compared to Cu. The importance of intermediate stabilization is reminiscent of the situation in the electrochemical reduction of CO on these two metals, where the lack of Au activity in the C-C coupling chemistry has been attributed to the weak CO binding, in contrast to the optimal Cu-CO binding energy allowing for coupled products.[51]

Spectroscopic Study of Dissociative Adsorption of Benzaldehyde on Pd and Pt Surfaces

Dissociative adsorption of benzaldehyde occurs upon its introduction to the Pd surface. Benzaldehyde is introduced to the electrolyte solution while holding the Pd electrode at -0.2 V. Unlike Au and Cu, the prominent features on Pd appear at 1717 and 1825 cm^{-1} upon introducing

1.5 mM of benzaldehyde (Figure 4A). We assign both peaks to adsorbed CO at the Pd surface. Although a band at 1713 cm^{-1} has been reported for benzaldehyde in cyclohexane,[57] such an assignment for the band centered at 1717 cm^{-1} is unlikely here. The 1717 cm^{-1} band is relatively broad and strengthens with time, whereas bands corresponding to the reactants are typically sharp and weaken over time due to consumption. Thus, it is more likely that the 1717 cm^{-1} band corresponds to an adsorbed formyl group and/or multibonded CO at defect sites (CO_M)[88] formed by the dissociative adsorption and decarbonylation of benzaldehyde. A similar CO_M peak has previously been observed between 1700 and 1740 cm^{-1} on Pd for low coverage of CO and during formic acid oxidation.[88] Importantly, in that study, the CO_M band appears only at low CO coverage, disappearing as the other CO peaks grow, in agreement with the 1717 cm^{-1} peak behavior at higher CO coverage (Figure 4B). The peak at 1825 cm^{-1} corresponds to CO adsorbed on Pd hollow sites (CO_H), and also forms via the decarbonylation of benzaldehyde. Similar decarbonylation induced CO peaks have been previously observed in thermochemical[57,89] and electrochemical[90] systems. Both the 1717 and 1825 cm^{-1} bands grow and blue shift with time, followed by the emergence of additional peaks at 1869 and 2009 cm^{-1}, corresponding to bridge and linearly bound CO, respectively $(CO_B$ and CO_L, respectively).[91] The sequential evolution of these bands suggests that benzaldehyde decarbonylates on defect and hollow sites, and the produced CO then migrates to bridge and linear binding sites (Scheme 2). This mechanism is similar to that suggested for benzaldehyde decarbonylation under thermocatalytic conditions.[89] Increasing the benzaldehyde concentration from 1.5 to 24 mM increases the CO_B and CO_L band intensities (Figure 4B). The growth in CO bands with higher benzaldehyde concentration suggests an initial undersaturation of CO by benzaldehyde decarbonylation at low benzaldehyde concentrations. To confirm the identity and stability of adsorbed CO, the potential is stepped anodically from -0.6 to 1.3 V, with spectra

collected every 0.1 V (Figure S11A). The adsorbed CO peaks shift with potential, with rates of 45, 51 and 36 cm^{-1}/V for CO$_L$, CO$_B$ and CO$_H$, respectively. These Stark tuning rates are consistent with the previously observed range for CO on Pd.[92] At 0.6 V, CO$_L$ oxidation begins, followed by CO$_B$ oxidation at 0.8 V and CO$_H$ at 0.9 V. The oxidation potentials generally agree with previous reports for CO on Pd,[93] supporting the CO peak assignments. No benzoate peak appears for Pd at higher potentials, suggesting more complete benzaldehyde oxidation than on Au.
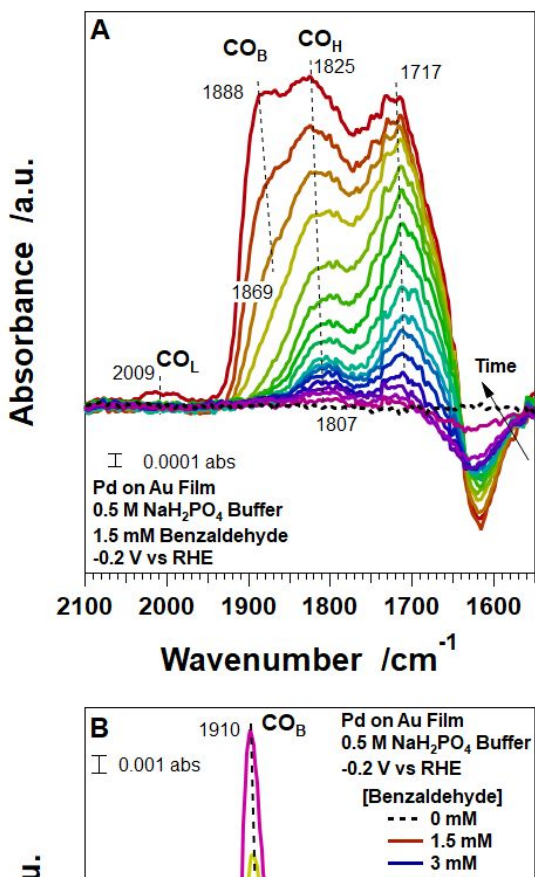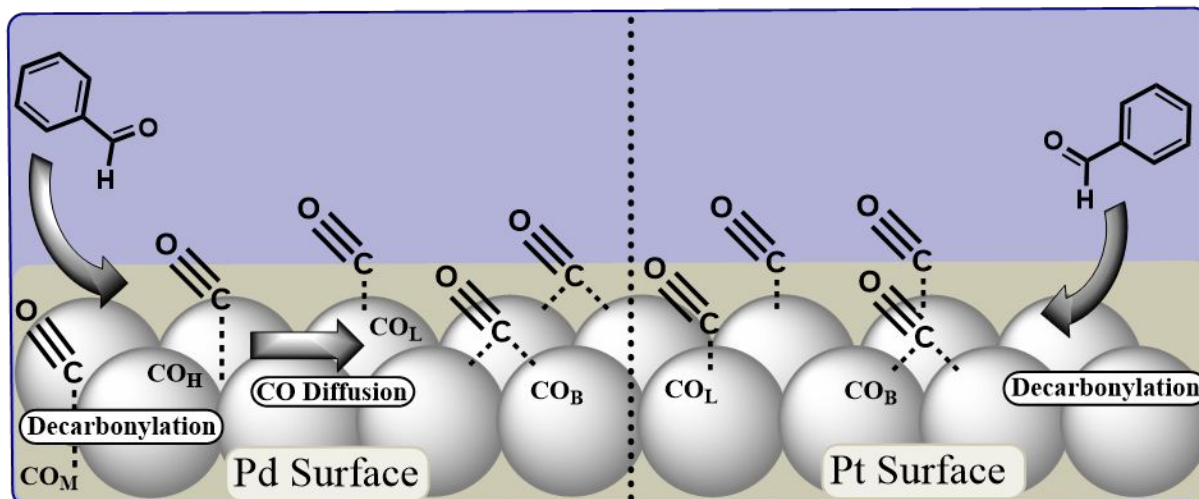
Scheme 2. Schematic representation for benzaldehyde decarbonylation on Pd and Pt. CO_M, CO_H, CO_B and CO_L stand for multi, hallow, bridge and linearly bonded CO, respectively.

CO poisoning by benzaldehyde decarbonylation on Pd is likely the main cause for its low dimerization selectivity in benzaldehyde reduction. Formation of CO on the Pd surface suggests instability of benzaldehyde at the Pd surface. Such instability agrees with the well-known ability of Pd to dissociative organic species,[94,95] a property usually attributed to strong back donation of electrons from the metal surface. For benzaldehyde, the destabilization likely results from back donation to the carbonyl π^* antibonding orbital, similar to other aldehydes.[94] This adsorbate instability and/or the resulting CO poisoning could then limit the formation of ketyl radicals near the catalyst surface. Given the suggested importance of these radicals for dimerization on Cu, the instability or poisoning may explain the lack of dimerization on Pd. Unfortunately, it is difficult to decouple the effects of the adsorbate instability and CO poisoning, as the former leads to the latter. However, the influence of potential can provide some insight into the relative importance of the two effects. If the ketyl radicals are unstable, reduction conditions may drive further decarbonylation at the surface, producing a potential dependence for CO formation. Such a potential dependence has been previously observed for benzaldehyde decarbonylation on Pt, with

CO peaks increasing at lower potentials.[81] Pd, however, does not show a similar dependence. Lowering the electrode potential from -0.2 to -0.5 V does not lead to any significant change in spectral features, except for the Stark tuning effect of the adsorbed CO bands (Figure 5A). The insensitivity of CO area to potential suggests that potential dependent species, such as ketyl radical intermediates, do not show a large degree of decomposition and that the primary decarbonylating species is likely benzaldehyde. Further, the small degree of ketyl radical decomposition may suggest some degree of stability for the radical, and that CO poisoning plays a greater role in preventing dimerization on Pd. Although the observed stability (lack of decomposition) also could be limited to decarbonylation, and the radicals remain relatively unstable compared to those on Cu or Au. To gauge the extent of CO poisoning on Pd, CO gas is introduced to the benzaldehyde saturated Pd surface at -0.5 V. The CO introduction results in blueshifts and a growth in intensity for both the CO_B and CO_L bands (Figure 5B), likely due to the increased CO coverage. This increase in CO coverage supports the incomplete saturation of CO by the decarbonylation process previously inferred from the CO dependence on benzaldehyde concentration (Figure 4). It can also provide a rough estimate for the extent of the initial CO poisoning. A linear relationship between CO peak area and coverage has been previously demonstrated for Pt in electrochemical systems[96] and used to quantify CO coverage on Pt and Pd in the presence of organic species.[90] Although others have suggested that dipole-dipole coupling may cause some deviation from linearity, particularly at high coverage, due to the screening of adjacent dipoles.[97–103] This deviation does not, however, appear very strong for Pt or Pd at intermediate coverage (below ~80-85% saturation).[101,104] We note that the introduction of CO increases the combined area of the CO_B and CO_L bands by ~40%. Assuming extinction coefficients independent of CO coverage, the increase suggests that decarbonylation poisons ~70% of the Pd surface relative to CO saturation. This

relatively large degree of poisoning, as well as its potential independence, suggests that CO poisoning is likely the primary cause for the lack of benzaldehyde coupling on Pd. It should be noted, however, that although the surface shows high CO coverage, the absolute magnitude of decarbonylation is quite limited. No benzene is detected either spectroscopically or by NMR, and the reaction is likely self-limiting as it produces a poisoning species (CO) which suppresses further propagation. Decarbonylation produced benzene has previously been detected for benzaldehyde on a Pt electrode using differential electrochemical mass spectrometry (DEMS),[81] a method with much higher sensitivity. The same study also lacked IR peaks for adsorbed benzene and suggested the exclusion of these bands by ATR selection rules due to a flat adsorption of the benzene molecule. A similar phenomenon may explain the lack of benzene in the present spectra for Pd (Figure 4A). We also note that the Pd spectra lack peaks corresponding to benzyl alcohol. The absence of these peaks likely results from low benzyl alcohol coverage due to the strong competitive adsorption of CO and benzaldehyde.
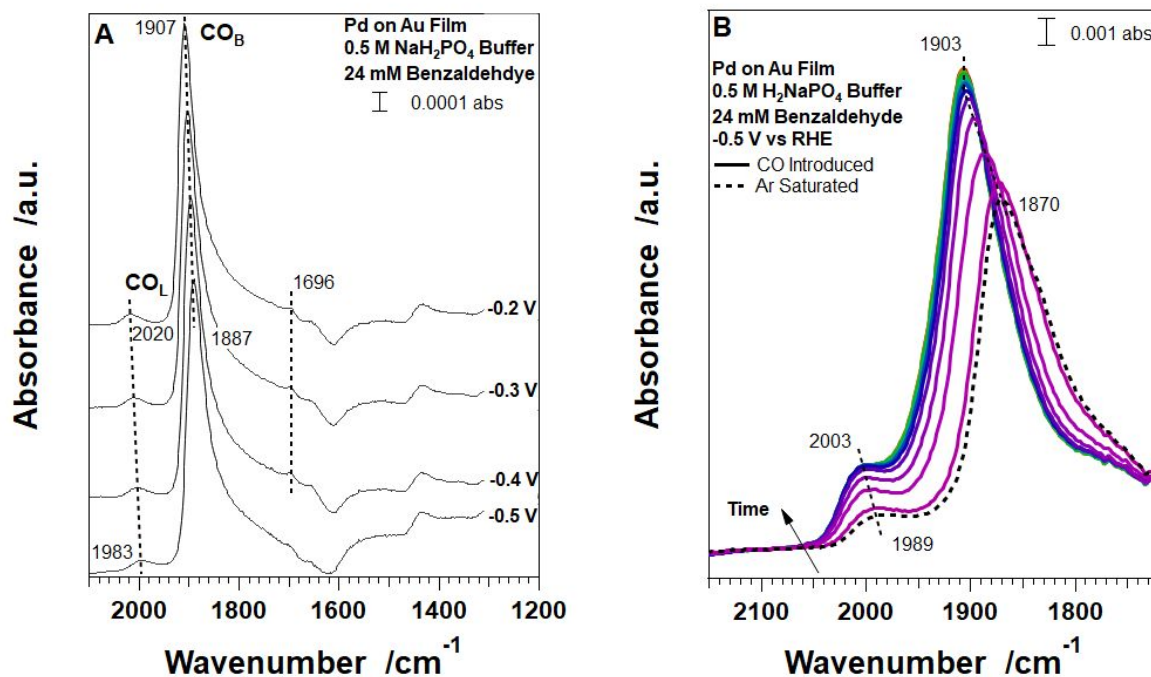
Figure 5. **(A)** Spectra collected for benzaldehyde saturated surface during downward potential steps on Pd. **(B)** Spectra collected upon the introduction of CO to benzaldehyde saturated Pd surface. Spectra were collected back to back. Backgrounds for both sets of spectra were collected at -0.2 V in pure buffer.

Similar to Pd, introduction of benzaldehyde to Pt also leads to dissociative adsorption, but with a different CO site distribution. At 1.5 mM benzaldehyde, benzaldehyde decarbonylation on Pt at 0 V results in a strong linear peak at 1977 cm^{-1}, with a weak bridge peak at 1754 cm^{-1} (Figure 6A) (Scheme 2). The Pt film requires a higher initial potential to avoid HER induced film instability due to its high HER activity (and the associated bubble formation). The CO formation agrees with previously observed benzaldehyde decarbonylation on Pt in aqueous electrochemical conditions below 0.2 V.[81,90] Both the linear and bridge CO peaks grow and blueshift with time as decarbonylation proceeds and CO coverage increases. Unfortunately, the near colinear evolution of the bands does not allow for determination of the decarbonylation site. However, recent work on similar poisoning during acetone reduction suggests the decarbonylation likely occurs at Pt (100) sites.[105] Increasing the benzaldehyde concentration primarily increases the CO$_L$ peak

intensity (Figure 6B). Unexpectedly, the CO_B peak intensity actually decreases slightly at higher benzaldehyde concentrations, suggesting either displacement of CO by benzaldehyde or that bridge sites become less energetically favorable at high coverages of the linearly bonded CO. At higher benzaldehyde concentrations, Pt also shows a small adsorbed benzaldehyde peak at 1689 cm^{-1}, a similar location to that on Au and Cu. The lower peak wavenumber on Pt likely results from interference by the adjacent water band. We note that the band corresponding to the radical species identified on Au and Cu does not appear on Pt. Like Pd, Pt also lacks bands attributable to benzyl alcohol, likely due to competitive benzaldehyde and CO adsorption. The adsorbed CO identity is confirmed by stepping the electrode potential to 1.3 V (Figure S11B). The CO_L and CO_B peaks both shift with potential, with Stark tuning rates of 32 and 61 cm^{-1}/V, respectively, similar to those previously observed for CO on Pt.[92] Similar to Pd, the CO on Pt peaks begin oxidizing at higher potentials. CO_B oxidizes at 0.8 V, followed by CO_L at 1 V, both generally consistent with the literature.[91,106]
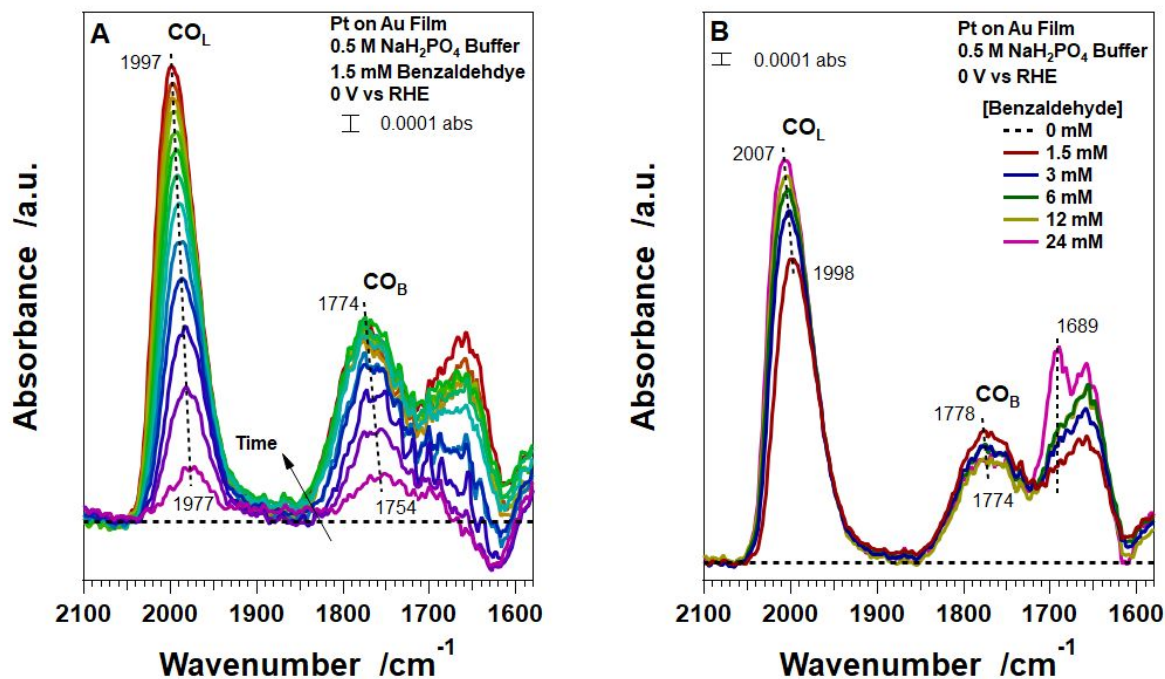
Figure 6. (A) Time evolution for benzaldehyde introduction to Pt. Spectra were collected ~3 min apart. **(B)** Effect of benzaldehyde concentration. Both sets of spectra were collected under Ar purge with a background at 0 V. CO_L, CO_B represent CO bound at linear and bridge sites, respectively.

The potential dependence of CO peak area on Pt suggests a greater role of radical instability in the benzaldehyde decarbonylation process than for Pd. Similar to Pd, the decarbonylation on Pt suggests instability of benzaldehyde adsorbates, which likely include ketyl radicals given the structural similarity to benzaldehyde, as evidenced by the spectra on Au and Cu (Figures 2 and 3). As discussed for Pd, these unstable radicals could also contribute to the formation of CO, and, depending on the relative stability of these radicals, decarbonylation may increase at lower potentials. To probe this possible influence of potential on adsorbate stability, the potential of the Pt surface is stepped from 0 to -0.2 V. Both the CO_L and CO_B peak intensities increase with the decreasing potential (Figure 7A). This trend runs counter to the CO_L peak decrease usually observed at lower potentials,[106,107] and agrees with the potential dependence previously observed for benzaldehyde decarbonylation on Pt.[81] This potential dependence suggests a greater

importance of the ketyl radical, in benzaldehyde decarbonylation on Pt and, as an extension, that the ketyl radicals are relatively unstable. This lower stability may suggest a greater role of ketyl radical stability in limiting coupling on Pt, especially compared to Pd, where benzaldehyde decomposition does not show potential dependence. However, we note that the observation of CO does indicate significant poisoning of the Pt surface. To gauge the extent of this poisoning, CO gas is introduced to the benzaldehyde saturated Pt surface at -0.2 V (Figure 7B). Upon introduction of CO, the CO_B peak grows slightly and blueshifts to 1815 cm^{-1}. Additionally, the CO_L peak at 2005 cm^{-1} shows slight growth and a blue shift, followed by the emergence of two new peaks at 2044 and 1985 cm^{-1}. These new peaks likely correspond to CO adsorbed in different chemical environments. The 2044 cm^{-1} peak agrees well with adsorption of CO_L on Pt,[93] and likely corresponds to areas of high CO-CO interaction. In contrast, the 1985 cm^{-1} peak represents a significant red shift, and likely results from CO interacting with benzaldehyde either adsorbed on or close to the surface. Such co-adsorption red shifts have been previously reported for CO on Pt in vacuum studies, with redshifts of 30 cm^{-1} for CO co-adsorbed with benzene[108] or methanol,[109] and 20 cm^{-1} for co-adsorption with water or Xe.[109] The effect has also been demonstrated in electrochemical systems, with 20 to 30 cm^{-1} red shifts for CO co-adsorbed with pyridine, CCl_4, or CS_2 at Pt and Pd electrodes.[110] Similarly, addition of water to CO adsorbed on a Pt electrode in acetonitrile results in a 30 cm^{-1} red shift in the CO peak.[111] Generally, these red shifts have been attributed to interactions between CO and the co-adsorbate, with CO dipole screening suggested as the most likely cause.[109,112] As an alternative theory to CO-benzaldehyde interactions, the new CO bands could also result from CO adsorbed at specific binding sites. In this view, the 2044 cm^{-1} peak would represent CO on Pt terraces,[113–115] with the 2005 and 1985 cm^{-1} peaks representing step[113–115] and undercoordinated[116,117] sites, respectively. These distinct CO adsorption sites have

been observed in thermocatalytic systems and some single crystal electrochemical studies.[113–116,118] Outside of single crystals, however, electrochemical studies generally observe only one, unresolved peak for CO_L on Pt.[81,106,107,119–121] This difficulty in observing distinct sites makes a site-specific interpretation unlikely, and the three distinct peaks more likely result from different degrees of CO-benzaldehyde interaction. Regardless of the cause, peak growth with CO introduction confirms the initial undersaturation of CO by decarbonylation on Pt. Similar to Pd, the change can also provide a rough estimate of the initial CO coverage. Specifically, the combined CO_L and CO_B peak areas increase by a factor of ~2 upon CO introduction, suggesting ~50% initial poisoning of the Pt surface by decarbonylation relative to CO saturation, assuming no significant change in extinction coefficient due to dipole-dipole coupling. This coverage is considerably lower than that measured for Pd, although the different potentials may account for some of the difference. Given the potential dependence for decarbonylation on Pt, the CO coverage likely increases at lower potentials, possibly surpassing that of Pd. Unfortunately, these lower potentials could not be probed directly due to the stability limitations of the Pt film used in the SEIRAS experiments. Such an increase in CO coverage might also explain why Pt shows a higher benzaldehyde reduction rate than Pd at -0.2 V, but the reverse is true at -0.5 V (Figure 1A).
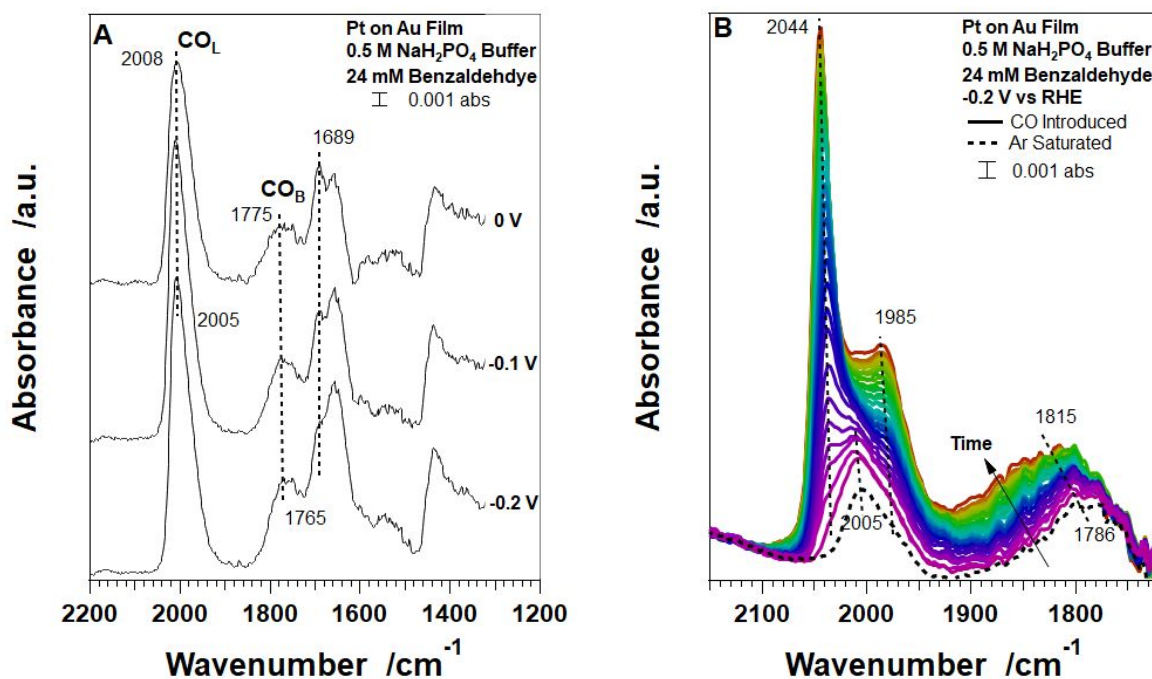
Figure 7. (A) Spectra collected during cathodic potential steps for a benzaldehyde adsorbed on a Pt surface. **(B)** CO introduction to the benzaldehyde saturated Pt surface. Spectra were collected back to back with no time delay. Backgrounds for both sets of spectra were collected at 0 V.

Radical Stability as a Predictor for Benzaldehyde Coupling Ability

Of the four metals investigated, Cu shows a unique ability to perform the coupling of benzaldehyde, which is attributable to a high stability and concentration of ketyl radical intermediates. Ketyl radical stability offers a framework for understanding the difference in benzaldehyde reduction selectivity between the alcohol selective metals of Pt, Pd and Au, and the unique coupling of Cu. Observation of ketyl radicals on Au (Figure 2), as well as previous electrochemical evidence,[34,38,40,43] suggests that these species are the main reaction intermediates in the electrochemical reduction of benzaldehyde. The concurrent evolution of these radicals and hydrobenzoin in the Cu spectra (Figure 3) suggests that hydrobenzoin formation requires the accumulation of ketyl radicals at or near the catalyst surface, with dimerization then occurring

through radical recombination, as suggested by previous studies.[25] However, this recombination does not occur to any appreciable extent on Au (< 0.2% FE), despite the presence of ketyl radicals. From the perspective of radical stability, this difference can be rationalized by a weaker stabilization of the radicals by Au compared to Cu. Such an explanation has an analog in the C-C coupling reactions which occur during the electrochemical reduction of CO. In these reactions, the difference between the effective coupling of Cu and the lack of coupling on Au has generally been attributed to the stronger CO binding energy of Cu compared to Au.[51] Radical stability can also rationalize the lack of benzaldehyde coupling for Pt and Pd. CO formation on Pd and Pt (Figures 4 and 6) suggests an instability of benzaldehyde adsorbates, which also likely extends to ketyl radical intermediates. The potential dependent decarbonylation for Pt but not Pd (Figures 5 and 7, respectively), may suggest greater radical stability for Pt, but in both cases the instability and resulting CO poisoning suggest a low concentration of ketyl radicals and no dimerization, as observed. Although the instability and CO poisoning do not completely suppress benzaldehyde reduction activity, as Pt and Pd still produce benzyl alcohol (Figure 1). In short, benzaldehyde and the ketyl radical bind too strongly to Pt and Pd, resulting in decomposition and poisoning in the extreme, and generally limiting radical accumulation and coupling. This radical stability formulation for Pd and Pt also finds an analog in electrochemical CO reduction, in which the lack of activity for Pd and Pt is linked to over-binding of CO.[51] Combining the Pd and Pt stability interpretation with that of Cu and Au offers a complete interpretation of the unique coupling on Cu. The Cu coupling results from its unique position as a catalyst active enough to produce sufficient radicals, but not so active as to destabilize intermediates and cause surface poisoning. In this regard, ketyl redical stability becomes analogous to CO binding energy in CO reduction and presents a general framework for understanding electroreductive coupling. In addition to

benzaldehyde, this framework could also rationalize and predict coupling activity for a broad range of carbonyl compounds. The effect of binding strength and specific intermediate structure could also be further explored given the strong adsorbate structure dependence recently suggested for acetaldehyde-CO coupling on Cu.[122] Additionally, the radical stability framework might be improved by extending investigations to identify the specific facets active for coupling on Cu and other coupling metals, as has been done for CO.[123] Alternatively, computational work might utilize ketyl radical stability for the design of optimum coupling catalysts, such as bimetallics, similar to previous work on hydrodeoxygenation catalysts.[124]

Conclusions

Batch reactivity studies show benzaldehyde reduction activity for Pt, and Pd at -0.2 V, and for Pt, Pd, Au, and Cu at -0.5 V. All four metals show the production of benzyl alcohol, however, only Cu shows the ability to effectively mediate the coupling of benzaldehyde to the hydrobenzoin dimer. ATR-SEIRAS results suggest that benzaldehyde adsorbs via the carbonyl carbon to the Au surface and is reduced to benzyl alcohol via a ketyl radical intermediate. Spectra on Cu further support the radical intermediate and suggest dimerization requires the accumulation of ketyl radicals. The lack of hydrobenzoin formation, despite radical formation, suggests the Au surface cannot accumulate radicals, likely due to poor stabilization relative to Cu. SEIRA spectra on Pd and Pt both show CO formation, suggesting unstable surface adsorbates under reducing conditions. The instability, and resulting CO poison, likely limit ketyl radical accumulation and prevent dimerization. On Pd, a higher CO coverage and lack of CO coverage potential dependence suggests a higher contribution from CO poisoning. On Pt, the lower coverage and potential dependence suggests a greater role of the intermediate instability. Based on the reactivity data and spectroscopic results, we propose that the ability of a catalyst to stabilize the ketyl radical

represents a key predictor in its ability to effectively mediate the electroreductive coupling of benzaldehyde, and likely other aromatic substrates with the carbonyl functional group.

Acknowledgements

References

1   N. M. Haegel, R. Margolis, T. Buonassisi, D. Feldman, A. Froitzheim, R. Garabedian, M. Green, S. Glunz, H.-M. Henning, B. Holder, I. Kaizuka, B. Kroposki, K. Matsubara, S. Niki, K. Sakurai, R. A. Schindler, W. Tumas, E. R. Weber, G. Wilson, M. Woodhouse and S. Kurtz, *Science (80-.).*, 2017, **356**, 141–143.

2   K. P. Kuhl, E. R. Cave, D. N. Abram and T. F. Jaramillo, *Energy Environ. Sci.*, 2012, **5**, 7050–7059.

3   L. Wang, S. A. Nitopi, E. Bertheussen, M. Orazov, C. G. Morales-Guio, X. Liu, D. C. Higgins, K. Chan, J. K. Nørskov, C. Hahn and T. F. Jaramillo, *ACS Catal.*, 2018, **8**, 7445–7454.

4   L. G. Feoktistov and H. Lund, in *Organic Electrochemistry an Introduction and Guide*, eds. M. Baizer and H. Lund, Marcel Dekker Inc, New York, NY, 2nd edn., 1983, pp. 315–348.

5   D. C. Elliott, *Curr. Opin. Chem. Eng.*, 2015, **9**, 59–65.

6   M. A. Kougioumtzis, A. Marianou, K. Atsonios, C. Michailof, N. Nikolopoulos, N. Koukouzas, K. Triantafyllidis, A. Lappas and E. Kakaras, *Waste and Biomass Valorization*, 2018, **9**, 2433–2445.

7   F. Camacho, P. González-Tello, E. Jurado and A. Robles, *J. Chem. Technol. Biotechnol.*, 1996, **67**, 350–356.

8   R. W. Torget, J. S. Kim and Y. Y. Lee, *Ind. Eng. Chem. Res.*, 2000, **39**, 2817–2825.

9   L. Liu, H. Liu, W. Huang, Y. He, W. Zhang, C. Wang and H. Lin, *J. Electroanal. Chem.*, 2017, **804**, 248–253.

10   Y. Kwon, E. De Jong, S. Raoufmoghaddam and M. T. M. Koper, *ChemSusChem*, 2013, **6**, 1659–1667.

11   Y. Kwon, Y. Y. Birdja, S. Raoufmoghaddam and M. T. M. Koper, *ChemSusChem*, 2015, **8**, 1745–1751.

12   S. Jung, A. N. Karaiskakis and E. J. Biddinger, *Catal. Today*, 2019, **323**, 26–34.

13   Y. Song, O. Y. Gutiérrez, J. Herranz and J. A. Lercher, *Appl. Catal. B Environ.*, 2016, **182**, 236–246.

14   X. H. Chadderdon, D. J. Chadderdon, J. E. Matthiesen, Y. Qiu, J. M. Carraher, J. P. Tessonnier and W. Li, *J.*

Am. Chem. Soc., 2017, **139**, 14120–14128.

15   L. A. Diaz, T. E. Lister, C. Rae and N. D. Wood, *ACS Sustain. Chem. Eng.*, 2018, **6**, 8458–8467.

16   H. D. Law, *J. Chem. Soc. Trans.*, 1906, 1512–1519.

17   H. D. Law, *J. Chem. Soc. Trans.*, 1906, **89**, 1520–1527.

18   H. D. Law, *J. Chem. Soc.*, 1907, **91**, 748.

19   H. D. Law, *J. Chem. Soc. Trans.*, 1911, **99**, 1113–1117.

20   Y. Song, U. Sanyal, D. Pangotra, J. D. Holladay, D. M. Camaioni, O. Y. Gutiérrez and J. A. Lercher, *J. Catal.*, 2018, **359**, 68–75.

21   U. Sanyal, J. Lopez-Ruiz, A. B. Padmaperuma, J. Holladay and O. Y. Gutiérrez, *Org. Process Res. Dev.*, 2018, **22**, 1590–1598.

22   J. A. Lopez-Ruiz, U. Sanyal, J. Egbert, O. Y. Gutiérrez and J. Holladay, *ACS Sustain. Chem. Eng.*, 2018, **6**, 16073–16085.

23   J. A. Lopez-Ruiz, E. M. Andrews, S. A. Akhade, M. Lee, K. Koh, S. F. Yuk, A. J. Karkamkar, M. A. Derewinski, J. Holladay, V. Glezakou, R. Rousseau, O. Y. Gutiérrez and J. D. Holladay, *ACS Catal.*, 2019, **9**, 9964–9972.

24   E. M. Andrews, J. A. Lopez-Ruiz, J. D. Egbert, K. Koh, U. Sanyal, M. Song, D. Li, A. J. Karkamkar, M. A. Derewinski, J. E. Holladay, O. Y. Gutiérrez and J. D. Holladay, *ACS Sustain. Chem. Eng.*, 2020, acssuschemeng.9b07041.

25   P. Zuman, *Electroanalysis*, 2006, **18**, 131–140.

26   A. M. Polcaro, S. Palmas and S. Dernini, *Electrochim. Acta*, 1993, **38**, 199–203.

27   J. Grimshaw and J. S. Ramsey, *J. Chem. Soc. C Org.*, 2004, 653.

28   P. Parpot, A. P. Bettencourt, G. Chamoulaud, K. B. Kokoh and E. M. Belgsir, *Electrochim. Acta*, 2004, **49**, 397–403.

29   Z. Li, S. Kelkar, L. Raycraft, M. Garedew, J. E. Jackson, D. J. Miller and C. M. Saffron, *Green Chem.*, 2014, **16**, 844–852.

30   P. Nilges and U. Schröder, *Energy Environ. Sci.*, 2013, **6**, 2925–2931.

31   L. Mandell, R. M. Powers and R. A. Day, *J. Am. Chem. Soc.*, 1958, **80**, 5284–5285.

32   J. H. Stocker and R. M. Jenevein, *J. Org. Chem.*, 1968, **33**, 294–297.

33   Y. Cao and T. Noël, *Org. Process Res. Dev.*, 2019, **23**, 403–408.

34   J. F. Rusling, J. P. Segretario and P. Zuman, *J. Electroanal. Chem. Interfacial Electrochem.*, 2006, **143**, 291–321.

35   M. K. Kalinowski, *Chem. Phys. Lett.*, 1971, **8**, 378–380.

36   S. Wawzonek and A. Gundersen, *J. Electrochem. Soc.*, 1960, **107**, 537–540.

37   F. Ammar, L. Nadjo and J. M. Saveant, *Electroanal. Chem. Interfacial Electrochem.*, 1973, **47**, 146–149.

38   L. Nadjo and J. M. Saveant, *J. Electroanal. Chem.*, 1971, **33**, 419–451.

39   P. Zuman, *Topics in Organic Polarography*, Plenum Publishing Company, Newyork, NY, 1970.

40   T. Guena and D. Pletch, *Acta Chem. Scand.*, 1998, **52**, 23–31.

41   A. Durant, H. François, J. Reisse and A. Kirsch-DeMesmaeker, *Electrochim. Acta*, 1996, **41**, 277–284.

42   M. Chandrasekaran, M. Noel and V. Krishnan, *J. Electroanal. Chem.*, 1991, **303**, 185–197.

43   S. G. Mairanolskil, T. Y. Rubinskaya, V. P. Gul'tyal and I. V. Proskurovskaya, *Bull. Acad. Sci. USSR, Div. Chem. Sci.*, 1976, **25**, 2360–2362.

44   V. J. Puglisi, G. L. Clapper and D. H. Evans, *Anal. Chem.*, 1969, **41**, 279–282.

45   Y. L. Chen and T. C. Chou, *J. Appl. Electrochem.*, 1994, **24**, 434–438.

46   M. D. Birkett and A. T. Kuhn, *Electrochem. Acta*, 1980, **25**, 273–278.

47   R. Udhayan and K. A. Basheer Ahamed, *B. Electrochem*, 1988, **4**, 163–165.

48   M. Vilar, J. L. Oliveira and M. Navarro, *Appl. Catal. A Gen.*, 2010, **372**, 1–7.

49   T. Chiba, M. Okimoto, H. Nagai and Y. Takata, *Chem. Soc. Japan*, 1982, **56**, 719–723.

50   Y. L. Chen and T. C. Chou, *Ind. Eng. Chem. Res.*, 1994, **33**, 676–680.

51   Y. Hori, 89–189.

52   G. Sandrock and G. Thomas, *Appl. Phys. A*, 2001, **72**, 153–155.

53   L. Schlapbach and A. Züttel, *Nature*, 2001, **414**, 353–358.

54   S. Jung and E. J. Biddinger, *ACS Sustain. Chem. Eng.*, 2016, **4**, 6500–6508.

55   A. S. May and E. J. Biddinger, *ACS Catal.*, , DOI:10.1021/acscatal.9b05531.

56   R. Zwarich, J. Smolarek and L. Goodman, *J. Mol. Spectrosc.*, 1971, **38**, 336–357.

57   C. Keresszegi, D. Ferri, T. Mallat and A. Baiker, *J. Phys. Chem. B*, 2005, **109**, 958–967.

58   NIST Spectrometry Data Center, in *NIST Chemistry WebBook, NIST Standard Reference Database Number 69*, eds. P. J. Linstrom and W. G. Mallard, National Institute of Science and Technology, Gaithersburg, MD.

59   M. Sankar, E. Nowicka, E. Carter, D. M. Murphy, D. W. Knight, D. Bethell and G. J. Hutchings, *Nat. Commun.*, 2014, **5**, 1–6.

60   A. Hatta, Y. Suzuki and W. Suëtaka, *Appl. Phys. A Solids Surfaces*, 1984, **35**, 135–140.

61   A. Hatta, Y. Chiba and W. Suëtaka, *Surf. Sci.*, 1985, **158**, 616–623.

62   A. Hatta, Y. Chiba and W. Suëtaka, *Appl. Surf. Sci.*, 1986, **25**, 327–332.

63   E. S. S. A, A. Hatta and W. Suetaka, *J. Electroanal. Chem.*, 1986, **215**, 93–102.

64   D. K. Lambert, *J. Chem. Phys.*, 1988, **89**, 3847–3860.

65   D. K. Lambert, *Electrochim. Acta*, 1996, **41**, 623–630.

66   D. Strmcnik, D. F. Van Der Vliet, K. C. Chang, V. Komanicky, K. Kodama, H. You, V. R. Stamenkovic and N. M. Marković, *J. Phys. Chem. Lett.*, 2011, **2**, 2733–2736.

67   C. A. Lucas, P. Thompson, Y. Gründer and N. M. Markovic, *Electrochem. commun.*, 2011, **13**, 1205–1208.

68   D. C. Cantu, A. B. Padmaperuma, M. T. Nguyen, S. A. Akhade, Y. Yoon, Y. G. Wang, M. S. Lee, V. A. Glezakou, R. Rousseau and M. A. Lilga, *ACS Catal.*, 2018, **8**, 7645–7658.

69   F. S. Tautz, *Prog. Surf. Sci.*, 2007, **82**, 479–520.

70   S. K. M. Henze, O. Bauer, T. L. Lee, M. Sokolowski and F. S. Tautz, *Surf. Sci.*, 2007, **601**, 1566–1573.

71   B. Schuler, W. Liu, A. Tkatchenko, N. Moll, G. Meyer, A. Mistry, D. Fox and L. Gross, *Phys. Rev. Lett.*, 2013, **111**, 1–5.

72   W. Liu, A. Tkatchenko and M. Scheffler, *Acc. Chem. Res.*, 2014, **47**, 3369–3377.

73   H. D. Abruna, J. H. White, M. J. Albarelli, G. M. Bommarito, M. J. Bedzyk and M. McMillan, *J. Phys. Chem.*, 1988, **92**, 7045–7052.

74   M. J. Bedzyk, D. Bilderback, J. White, H. D. Abruña and M. G. Bommarito, *J. Phys. Chem.*, 1986, **90**, 4926–4928.

75   H. V. K. Udupa, G. S. Subramanian, K. S. Udupa and K. Natarajan, *Electrochim. Acta*, 1964, **9**, 313–323.

76   D. R. Tallant and D. H. Evans, *Anal. Chem.*, 1969, **2**, 835–838.

77   D. H. Eargle, *J. Org. Chem.*, 1974, **39**, 1295–1297.

78   D. H. Eargle and R. Emrich, *J. Org. Chem.*, 1970, **35**, 3744–3747.

79   D. H. Eargle, *J. Chem. Soc. B Phys. Org.*, 1970, **1966**, 1556–1560.

80   A. Bewick, W. Jones and M. Kalaji, *Electrochem. Acta*, 1996, **41**, 1961–1970.

81   G. A. Planes, E. Moran, J. L. Rodriguez, C. Barbero and E. Pastor, *Langmuir*, 2003, **19**, 8899–8906.

82   P. Gao and M. J. Weaver, *J. Phys. Chem.*, 1985, **89**, 5040–5046.

83   P. Yankov, Z. Nickolov, V. Zhelyaskov and I. Petkov, *J. Photochem. Photobiol. A Chem.*, 1989, **47**, 155–165.

84   S. Solar, N. Getoff, J. Holcman and K. Sehested, *J. Phys. Chem.*, 1995, **99**, 9425–9429.

85   N. Steinberger and G. K. Fraenkel, *J. Chem. Phys.*, 1964, **40**, 723–729.

86   R. Wilson, *Can. J. Chem.*, 1966, **44**, 551–559.

87   P. H. Rieger and G. K. Fraenkel, *J. Chem. Phys.*, 1962, **37**, 2811–2831.

88   H. Miyake, T. Okada, G. Samjeske and M. Osawa, *Phys. Chem. Chem. Phys.*, 2008, **10**, 3607–3608.

89   D. Ferri, C. Mondelli, F. Krumeich and A. Baiker, *J. Phys. Chem. B*, 2006, **110**, 22982–22986.

90   L. W. H. Leung and M. J. Weaver, *Langmuir*, 1990, **6**, 323–333.

91   Y. G. Yan, Q. X. Li, S. J. Huo, M. Ma, W. Bin Cai and M. Osawa, *J. Phys. Chem. B*, 2005, **109**, 7900–7906.

92   M. J. Weaver, S. Zou and C. Tang, *J. Chem. Phys.*, 1999, **111**, 368–381.

93   H. Miyake, E. Hosono, M. Osawa and T. Okada, *Chem. Phys. Lett.*, 2006, **428**, 451–456.

94   R. Shekhar, M. A. Barteau, R. V Plank and J. M. Vohs, *J. Phys. Chem. B*, 1997, **101**, 7939–7951.

95   H. Baltruschat and U. Schmiemann, *Ber. Bunsengers. Phys. Chem.*, 1993, **97**, 452–460.

96   D. S. Corrigan and M. J. Weaver, *J. Electroanal. Chem.*, 1988, **241**, 143–162.

97   B. N. J. Persson and R. Ryberg, *Phys. Rev. B*, 1981, **24**, 6954–6970.

98   E. Schweizer, B. N. J. Persson, M. Tushaus, D. Hodge and A. M. Bradshaw, *Surf. Sci.*, 1989, **213**, 49–89.

99   B. E. Hayden and A. M. Bradshaw, *Surf. Sci.*, 1983, **125**, 787–802.

100   P. Hollins and J. Pritchard, *Prog. Surf. Sci.*, 1985, **19**, 275–349.

101   K. Kunimatsu, *J. Electroanal. Chem.*, 1986, **213**, 149–157.

102   M. W. Severson, C. Stuhlmann, I. Villegas and M. J. Weaver, *J. Chem. Phys.*, 1995, **103**, 9832–9843.

103   B. N. J. Persson and A. Liebsch, *Surf. Sci.*, 1981, **110**, 356–368.

104   A. Ortega, F. M. Hoffman and A. M. Bradshaw, *Surf. Sci.*, 1982, **119**, 79–94.

105   C. J. Bondue, F. Calle-vallejo, M. C. Figueiredo and M. T. M. Koper, *Nat. Catal.*, , DOI:10.1038/s41929-019-0229-3.

106   M. Dunwell, J. Wang, Y. Yan and B. Xu, *Phys. Chem. Chem. Phys.*, 2017, **19**, 971–975.

107   Y. Ikezawa, H. Saito, H. Matsubayashi and G. Toda, *J. Electroanal. Chem.*, 1988, **252**, 395–402.

108   R. W. Ittner and H. Luth, *Stud. Surf. Sci. Catal.*, 1981, **7**, 95–107.

109   D. H. Ehlers, A. P. Esser, A. Spitzer and H. Lüth, *Surf. Sci.*, 2010, **191**, 466–478.

110   M. Dunwell, Y. Yan and B. Xu, *ACS Catal.*, 2017, **7**, 5410–5419.

111   S. Hoffer, S. Baldelli, K. Chou, P. Ross and G. A. Somorjai, *J. Phys. Chem. B*, 2002, **106**, 6473–6478.

112   H. Moritz and H. Lüth, *Vacuum*, 1990, **41**, 63–64.

113   C. S. Kim, W. J. Tornquist and C. Korzeniewski, *J. Phys. Chem.*, 2005, **97**, 6484–6491.

114   J. Xu, P. Henriksen and J. T. Yates, *J. Chem. Phys.*, 1992, **97**, 5250–5252.

115   C. S. Kim, C. Korzeniewski and W. J. Tornquist, *J. Chem. Phys.*, 1994, **100**, 628–630.

116   L. DeRita, S. Dai, K. Lopez-Zepeda, N. Pham, G. W. Graham, X. Pan and P. Christopher, *J. Am. Chem. Soc.*, 2017, **139**, 14150–14165.

117   M. J. Kappers and J. H. van der Maas, *Catal. Letters*, 1991, **10**, 365–374.

118   S. Watanabe, Y. Kinomoto, F. Kitamura, M. Takahashi and M. Ito, *J. Electron Spectro.*, 1990, **54–55**, 1205–1214.

119   G. Q. Lu, S. G. Sun, L. R. Cai, S. P. Chen, Z. W. Tian and K. K. Shiu, *Langmuir*, 2000, **16**, 778–786.

120   K. Kunimatsu, W. G. Golden, H. Seki and M. R. Philpott, *Langmuir*, 1985, **1**, 245–250.

121   A. E. Bjerke, P. R. Griffiths and W. Theiss, *Anal. Chem.*, 1999, **71**, 1967–1974.

122   X. Chang, A. Malkani, X. Yang and B. Xu, *J. Am. Chem. Soc.*, 2020, **142**, 2975–2983.

123   K. Jiang, R. B. Sandberg, A. J. Akey, X. Liu, D. C. Bell, J. K. Nørskov, K. Chan and H. Wang, *Nat. Catal.*, 2018, **1**, 111–119.

124   F. Jalid, T. S. Khan, F. Q. Mir and M. A. Haider, *J. Catal.*, 2017, **353**, 265–273.